Published online 26 April 2023

Nucleic Acids Research, 2023, Vol. 51, No. 12 ***5981–5996***
https://doi.org/10.1093/nar/gkad271

Progesterone receptor mediates ovulatory transcription through RUNX transcription factor interactions and chromatin remodelling

Doan T. Dinh[1,*], James Breen[2,3], Barbara Nicol[4], Natalie J. Foot[1], David C. Bersten[1], Alaknanda Emery[1], Kirsten M. Smith[1], Ying Y. Wong[1], Simon C. Barry[1], Humphrey H.C. Yao[4], Rebecca L. Robker[1] and Darryl L. Russell[1,*]

[1]Robinson Research Institute, School of Biomedicine, Faculty of Health & Medical Sciences, University of Adelaide, Australia, [2]Indigenous Genomics, Telethon Kids Institute, Adelaide, Australia, [3]College of Health & Medicine, Australian National University, Canberra, Australia and [4]Reproductive Developmental Biology Group, National Institute of Environmental Health Sciences, Research Triangle Park, NC 27709, USA

Received August 15, 2022; Revised March 30, 2023; Editorial Decision April 01, 2023; Accepted April 19, 2023

ABSTRACT

Progesterone receptor (PGR) plays diverse roles in reproductive tissues and thus coordinates mammalian fertility. In the ovary, rapid acute induction of PGR is the key determinant of ovulation through transcriptional control of a unique set of genes that culminates in follicle rupture. However, the molecular mechanisms for this specialized PGR function in ovulation is poorly understood. We have assembled a detailed genomic profile of PGR action through combined ATAC-seq, RNA-seq and ChIP-seq analysis in wildtype and isoform-specific PGR null mice. We demonstrate that stimulating ovulation rapidly reprograms chromatin accessibility in two-thirds of sites, correlating with altered gene expression. An ovary-specific PGR action involving interaction with RUNX transcription factors was observed with 70% of PGR-bound regions also bound by RUNX1. These transcriptional complexes direct PGR binding to proximal promoter regions. Additionally, direct PGR binding to the canonical NR3C motif enable chromatin accessibility. Together these PGR actions mediate induction of essential ovulatory genes. Our findings highlight a novel PGR transcriptional mechanism specific to ovulation, providing new targets for infertility treatments or new contraceptives that block ovulation.

GRAPHICAL ABSTRACT

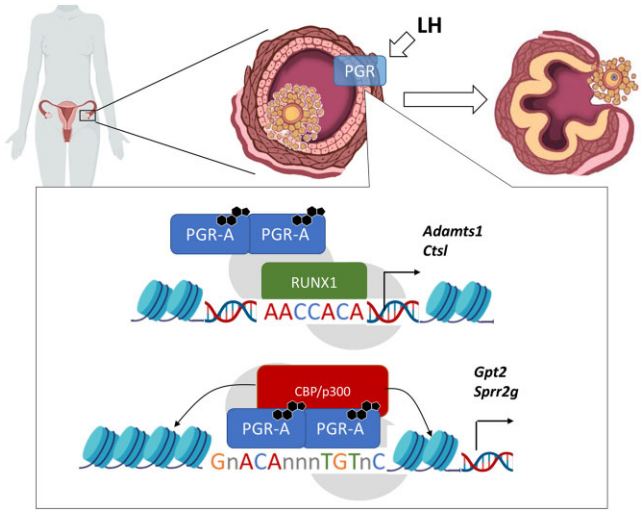

INTRODUCTION

Ovulation is a highly controlled tissue remodelling process that ensures the release of appropriately mature oocytes from the ovary, timed to coincide with the receptivity of the uterus for embryo implantation. The mechanism of ovulation begins with a surge of luteinizing hormone (LH) from the pituitary that acts on ovarian granulosa cells to cause pervasive reprogramming of gene expression, structural remodelling of the ovarian follicle and the resumption of oocyte meiotic maturation (1,2).

Progesterone signalling through progesterone receptor (PGR) is an obligatory transcriptional regulator in granulosa cells mediating ovulation (3,4), while coincidently pro-

*To whom correspondence should be addressed. Tel: +61 883134096; Email: darryl.russell@adelaide.edu.au
Correspondence may also be addressed to Doan T. Dinh. Email: doan.dinh@adelaide.edu.au

moting uterine receptivity, lactation in the mammary gland, and many other roles, making PGR a diverse critical regulator of female fertility. PGR expression is induced by the LH-surge and is activated through endogenous progesterone, which is locally synthesised by the highly steroidogenic granulosa cells throughout the majority of the oestrus cycle (5). However, the tissue-specific molecular interactome of PGR and the mechanism through which PGR induces genes that are essential for follicular rupture and the release of oocytes is not known. Female mice with either total or granulosa-specific null mutation of the nuclear PGR have a complete anovulatory phenotype without affecting oocyte meiosis or follicle luteinization (3,4,6). Likewise, in primates and humans, administration of PGR antagonists (mifepristone or ulipristal acetate) blocks ovulation (7,8). However, disrupting systemic progesterone action has side effects across target organs, necessitating further research into the unique ovarian PGR action and its downstream target genes in order to understand fertility regulation and discover selective targets for ovulation-blocking contraceptives.

As a steroid receptor belonging to the NR3C family, PGR is a ligand activated nuclear transcription factor. The classical PGR action involves ligand-activated binding of the NR3C response element (minimally ACAnnnTGT), which activates target gene transcription. However, this classic model does not explain the complexity of diverse actions of PGR in its many target tissues. Furthermore, as the NR3C motif is also recognized by other steroid receptors, other non-canonical mechanisms are required to allow for hormone and tissue-specific transcriptional regulation by steroid receptors. PGR-chromatin interaction and transcriptional induction is highly intricate and involves cooperation with specific transcription factors in different cellular contexts (9,10). The transcriptional complex can recruit histone and chromatin remodellers including steroid receptor coactivators (SRC), CBP/p300 and PRMT1 (11–13) to facilitate accessibility for the basal transcriptional machinery and RNA Pol II to induce expression of target genes (14). PGR isoforms provide some functional specificity, including distinct protein-protein interaction capabilities (15), as demonstrated by repression of PGR-B transcriptional activity by PGR-A in the uterus (16) and breast cancer cells (17). In the ovary, both PGR isoforms are induced by the LH surge (18,19); however, PGR-A is credited as the more essential isoform in ovulation, as shown through PGR-A specific KO mouse model (AKO) (20). In contrast, female mice lacking only PGR-B (BKO) exhibit normal ovulation (21). The relative importance of PGR-A and PGR-B throughout reproductive physiology remains an active topic of investigation (22–24), and their molecular mechanisms in granulosa cells that control ovulation remain unknown.

Our previous characterization of the granulosa cell PGR cistrome through ChIP-seq suggests that the classic pathway involving PGR binding the canonical NR3C motif is not favoured by PGR in this context. Instead, PGR-bound sites in granulosa cells are specifically enriched for the RUNX-binding RUNT motif (19). Here we performed a comprehensive analysis of LH- and PGR-driven transcriptomes and chromatin accessibility through RNA-seq and ATAC-seq in wildtype, PGR null and isoform-specific PGR mutant mouse granulosa cells stimulated *in vivo*. This defined the remarkably acute and pervasive change in transcriptional and accessible chromatin landscapes induced by the LH surge and PGR. To understand the tissue-specific mechanisms of PGR action in mediating ovulatory gene expression patterns, we performed comparative ChIP-seq analyses along with proximity ligation assay and immunoprecipitation-mass spectrometry to identify the physical interaction between PGR and RUNX1. The results establish a new molecular model for tissue-specific PGR action involving PGR and RUNX1 co-operativity to shape granulosa cell chromatin epigenetic reprogramming and transcriptional response to the LH surge.

MATERIALS AND METHODS

Reagents and antibodies

Unless otherwise stated, reagents were purchased from Sigma-Aldrich (St. Louis, MO, USA).

Animals

21-day old CBA × C57BL/6 F1 (CBAF1) mice were obtained from the Laboratory Animal Services (University of Adelaide). Null mutant mouse strains with ablation of either all PGR isoforms, or specific ablation of PGR-A or PGR-B (6,20,21) were obtained from the Jackson Laboratory (Bar Harbor, USA). PGRKO mice are a targeted mutation strain with the Jackson Laboratory designation Pgr^{tm1Bwo}. PGR-A KO (AKO) mice are a targeted mutation strain with the Jackson Laboratory designation Pgr^{tm1Omc}. PGR-B KO (BKO) mice are a targeted mutation strain with the Jackson Laboratory designation Pgr^{tm2Omc}. Mice from KO strains are routinely genotyped from ear or tail biopsies before allocation to experiments and confirmed from replicate biopsies collected at the time of experiments. All mice were maintained in 12 h light/12 h dark conditions and given water and rodent chow *ad libitum*. Littermate females of each genotype were allocated for experiments at 21 days of age. All experiments were approved by The University of Adelaide Animal Ethics Committee and were conducted in accordance with the Australian Code of Practice for the Care and Use of Animals for Scientific Purposes (ethics number m/2015/075, m/2018/100, m/2018/122, m/2018/117).

Granulosa cell culture and hormone treatment

CBAF1 female mice were stimulated with 5 IU eCG (Lee BioSolutions, Maryland Heights, USA) and culled at 44 h post-eCG, upon which ovaries were dissected and granulosa cells isolated. Cumulus-oocyte complexes were removed and granulosa cells were counted before being seeded into an 8-well fibronectin-coated chamber slide (minimum 100 000 cells/well). Cells were cultured in DMEM:F12 media (Thermo Fisher) at 37ºC, 5% CO_2 for 90 min then washed with PBS to remove debris. Cells were incubated overnight and were treated with 2 IU/ml hCG (Merck Sharp & Dohme B.V., Haarlem, Netherlands) and 100 nM R5020 (PerkinElmer, Waltham, USA) for indicated durations at 37ºC, 5% CO_2.

ATAC-seq

ATAC-seq was performed as previously described (25). Briefly, granulosa cells were collected from superovulated female CBAF1 or PGRKO mice at 0 h or 6 h post-hCG as above. Cells from 2–3 animals were pooled together for one biological replicate, two replicates were obtained per condition. Granulosa cells were lysed and tagmentation was performed on the nuclei using the Illumina Tagment DNA TDE1 Enzyme and Buffer Kits (Illumina, San Diego, USA). DNA purification was performed using the Monarch PCR & DNA Cleanup Kit (NEB, Ipswich, USA). Libraries were then amplified and purified before being size selected using magnetic AMPure XP Beads (Beckman Coulter, Brea, USA). Library fragmentation was confirmed using the LabChIP GX Bioanalyser (PerkinElmer) and sequencing was performed on the HiSeq2500 Sequencing System (Illumina). For all datasets, adapters were trimmed from 150-base sequences using Cutadapt (26) and aligned to the mm10 mouse genome using Bowtie2 algorithm (27). Alignment was filtered using samtools for non-mitochondrial reads with MAPQ $\geq$30 cut-off and was deduplicated using Picard tools. Peak calling from read count followed the algorithm for Model-based Analysis for ChIP-Seq (MACS2) with a q-value cut-off = 10^{-10} and a mouse genome size of 1.87×10^9 (28). Differential binding analysis for LH ATAC-seq and PGR ATAC-seq was performed using DiffBind (29) with DESeq2 linear model, with differentially enriched sites determined to have FDR $\leq$0.05. Spearman correlation between biological replicates was assessed using deepTools (Supplementary Figure S8A-B) (30). Genomic distribution of peak subsets was determined using the ChIPseeker package (31). Gene ontology enrichment analysis was performed using GREAT (32). Differential enrichment of transcription factor binding motif and DNA footprinting analysis was performed using TOBIAS (33). Motif analysis for *de novo* sequence motifs was performed using HOMER motif finding algorithm with random 200 bp-long sequences from the mouse genome used to estimate motif frequency in random sequence (34). Visual representation of ATAC signal was through the UCSC Genome Browser (Santa Cruz, USA).

RNA-seq

Three-week old female mice, either CBAF1 (for LH RNA-seq) or WT and KO from PGRKO, AKO and BKO strains (for PGR RNA-seq) were hormonally stimulated as above, before being culled at 8 h post-hCG injection for granulosa cell collection. For LH RNA-seq, eCG-treated mice that did not receive hCG injection served as negative control. For each condition, four biological replicates were collected, each containing cells pooled from three individual animals. RNA was extracted from granulosa cells using RNeasy Mini kit (Qiagen, Chadstone, VIC, Australia). RNA quality was assessed using the RNA ScreenTape System (Agilent, Santa Clara, CA, USA).

For LH response RNA-seq, RNA was subjected to rRNA depletion using a modified Ribozero method and library preparation using Clontech SMARTer Stranded RNA-Seq Kits (Takara Bio, Shiga, Japan). Sequencing was performed on the Illumina HiSeq2500 100bp PE Rapid run (Ramaciotti Centre for Genomics, Kensington, Australia). For PGR RNA-seq, the library was prepared using the Universal RNA-Seq library kit with NuQuant Mouse AnyDeplete (Nugen, Redwood City, USA) and sequencing was performed on the NovaSeq 6000 S1 Sequencing System (South Australian Health & Medical Research Institute, Adelaide, Australia). Over-represented adapters were checked using FastQC (https://www.bioinformatics.babraham.ac.uk/projects/fastqc/) and adapters were trimmed using AdapterRemoval (35) when required. Quasi-aligment of each dataset to the GENCODE mouse transcriptome (GRCm38.p6, M25 release) and transcript quantification were through Salmon (36). Expression profiles and differential gene expression were assessed with limma (37) and edgeR (38) using mean-variance estimates from log counts as described in the limma voom method. Differential gene expression for each experiment was defined as a fold-change $\geq$ 2 ($|\log FC| \geq 1$) and Benjamini–Hochberg adjusted *P*-value $\leq$ 0.01. Upstream regulator analysis of DEGs was through IPA software (QIAGEN). For visualization of RNA-seq on the UCSC Genome Browser, read coverage was processed using deepTools (30).

ChIP-seq

Granulosa cells from CBAF1 female mice were collected by puncturing ovarian follicles 44 h after eCG (0 h hCG) and 6 h after hCG stimulation. Two biological replicates were obtained for each sample from 10 mice, each with at least 1×10^7 cells. ChIP-seq for RUNX1 was performed by Active Motif (Carlsbad, USA) as previously described (19) using in-house RUNX1 antibody (39). For all datasets, sequences were aligned to the mm10 mouse genome using Bowtie2 algorithm. Peak calling from read count followed the algorithm for MACS2 with a p-value cut-off = 10^{-10}. Overlapped peaks determined using the ChIPpeakAnno package (40) were used as the consensus data in all subsequent comparisons. Genomic distribution was performed using the ChIPseeker package. Spearman correlation between biological replicates was assessed using deepTools (Supplementary Figure S8C) (30). Differential binding analysis for RUNX1 ChIP-seq was performed using DiffBind as described above. Peak characterization was determined using the ChIPseeker package. Motif analysis for known and *de novo* sequence motifs was performed using HOMER as described above. Visualization of ChIP-seq signal was through the UCSC Genome Browser. For estimation of PGR binding affinity at ChIP peaks, a quantitative DNA binding model of NR3C from AR Round 1–4 HT-SELEX data (41,42) was generated using the No Read Left Behind tool (NRLB) (43). The AR round-4 15mer dinucletotide model (index 22) (Supplementary Figure S6A) was selected for energy logo motif representation and scoring of DNA sequences. All possible offsets of the 15mer sequence within each PGR ChIP peak or randomly selected genomic regions (350 bp) were scored using FASTscoreBED.indx (44) and the Area Under the Curve (AUC) for each DNA region was calculated. pROC (45) was used to generate the ROC.

Integration of chromatin capture data

Mouse granulosa cell Hi-C data (46) and human ovary promoter capture-C data (47) was obtained from associated GEO entries. For Hi-C data, contact matrix as processed in (46) was obtained and statistically significant chromatin loops at 10 kb bin and P-value = 0.05 threshold were determined through HiCExplorer tools (48). Chromatin loops were annotated to mouse genes using the org.Mm.eg.db package (49) or overlapped with PGR and RUNX1 ChIP-seq peaks using the ChIPpeakAnno package. For capture-C data, hg19 coordinates of loops called in the original publication for human ovary were converted to mm10 using liftOver utility (UCSC toolkit) (50) at 50% nucleotide matching criteria, then annotated and overlapped with PGR ChIP-seq data. Visualization of integrated data was through the UCSC Genome Browser.

Proximity ligation assay (PLA)

PLA was performed on cultured granulosa cells using the Duolink PLA Probes and PLA Fluorescence *in situ* Detection Kit Red (Sigma) following the manufacturer's protocol. Briefly, cultured granulosa cells were fixed in 4% paraformaldehyde and permeabilized with PBS + 0.01% Triton X-100 for 1 h at room temperature. Cells were blocked with Blocking Buffer for 1 h at 37ºC and incubated with primary antibody couples (PGR – Cell Signalling Technology (CST), #8757; RUNX1 – Santa Cruz Biotechnology (SCB), #sc-365644; RUNX2 – SCB, #sc-390715; c-JUN – SCB, # sc-376488; JUNB – SCB, #sc-8051; JUND – SCB, #sc-271938; LRH1 – Perseus Protemics, #PP-H2325-00, CBP/p300 – CST, #7389) diluted in Antibody Diluent for 2 h at room temperature or overnight at 4ºC. Then, cells were incubated with PLA probes of appropriate species for 1 h at 37ºC, oligo probes were ligated for 30 min at 37ºC and the amplification reaction was at 37ºC for a minimum of 100 min. Between steps, cells were washed using the provided wash buffers. Slides were mounted with Prolong Gold Mounting Media with DAPI (Thermo Fisher), cured for at least 1 h in the dark and were stored at –20ºC prior to imaging by Olympus confocal microscope. The nuclear boundary for each cell was determined through DAPI staining. PLA signals were identified as fluorescent puncta in the nucleus and quantified using the 'Count Maxima' function in ImageJ for each cellular compartment. Significant differences between time points were determined through one-way ANOVA with Tukey test for multiple comparison.

GFP-trap immunoprecipitation and mass spectrometry

KGN human granulosa cells were grown in Dulbecco's modified Eagle's medium/Ham's F12 nutrient mix (DMEM/F12) supplemented with 10% fetal calf serum, 0.5 M HEPES and 100 units/ml penicillin-streptomycin at 37°C with 10% CO_2. Cells were infected with GFP-tagged PGR-A (or GFP alone as control) in the lentiviral vector pLV-TRE3G-GtwyA-EF-Tet-On3G-P2A-puro, and stably selected using puromycin. Gene expression was induced by the addition of doxycycline 24 h prior to harvest. On the day of experiment, cells were treated with 100 nM R5020 for 4 h. Cells were then trypsinised and resuspended in HEPES buffered saline (40 mM HEPES pH 8.05, 150 mM NaCl) before being cross-linked with 1 mg/ml Dithiobis(succinimidyl propionate) (DSP) for 2 min with gentle rocking. 100 mM Tris–HCl (pH 8.0) was then added to cells to quench the DSP followed by washing in cold PBS. Cells were then lysed in lysis buffer (40 mM HEPES, 1% Triton X-100, 150 mM NaCl, 2.5 mM $MgCl_2$, 2 mM EDTA, 0.85% Igepal/NP-40, HALT protease and phosphatase inhibitors (Thermo Fisher), 50 μM PR-619 DUB inhibitor) at 4°C for 30 min, followed by removal of cell debris by centrifugation at 14 000 rpm for 2 min at 4°C. Protein complexes were then immunoprecipitated using GFP-Trap magnetic agarose beads (ProteinTech, Rosemont, USA), incubating overnight at 4°C with gentle rocking. The following day, beads were washed five times in lysis buffer, then once in PBS and protein complexes eluted in 3 × 50 μl 0.1 M glycine pH 2.5 then neutralised with 30 μl of 1 M Tris–HCl pH 9.

GFP-Trap pulldowns were subjected to quantitative label-free based mass spectrometry analysis using a DIA-MS approach, performed at the Walter and Eliza Hall Institute (Melbourne, Australia). Briefly, the eluted protein material was subjected to FASP digestion prior to peptide separation using a 30-min linear gradient on a timsTOF pro MS (Bruker) using data independent acquisition (DIA) in diaPASEF mode. These data were subsequently searched on DIA-NN software in a library-free approach. Differential expression analysis was performed using limma (v. 3.52.4). A protein was determined to be significantly differentially expressed if the $\log_2$ fold change was ≥1 and exhibited an adjusted P-value ≤0.05 after Benjamini-Hochberg correction.

RESULTS

Ovulatory stimulus reprograms chromatin state and transcription through distinct transcription factor binding

Ovulation induction by hCG injection in mice provides an *in vivo* model for the rapid response to ovulatory cues in granulosa cells. Comparative ATAC-seq revealed dynamic changes in chromatin accessibility and ovulatory transcription factor binding. Stringent ATAC-seq peak calling criteria identified a total of 71 287 accessible chromatin peaks, over two-thirds of which were modified within 6 h of LH stimulus, 28 729 sites (40.3%) were LH-induced, 21 257 sites (29.8%) were significantly repressed and 21 301 sites (29.8%) with no change in accessibility (FDR ≤ 0.05, Figure 1A). LH-mediated change in accessibility occurred not only in promoters but also at distal enhancers and throughout gene bodies (Figure 1B). LH induced accessibility corresponded to genes involved in cytoskeletal reorganization, mitochondrial functions, and signalling pathway activation which are important processes leading up to ovulation, while significantly, LH reduced open chromatin near genes that were responsible for gene silencing and nucleosome modification (Supplementary Figure S1).

To predict the activity of key transcription factors involved in changes in the accessibility of LH-mediated open chromatin sites, differential analysis of transcription factor binding motifs was performed (Figure 1C, Supplementary Table S1). The motif for many known ovulatory tran-

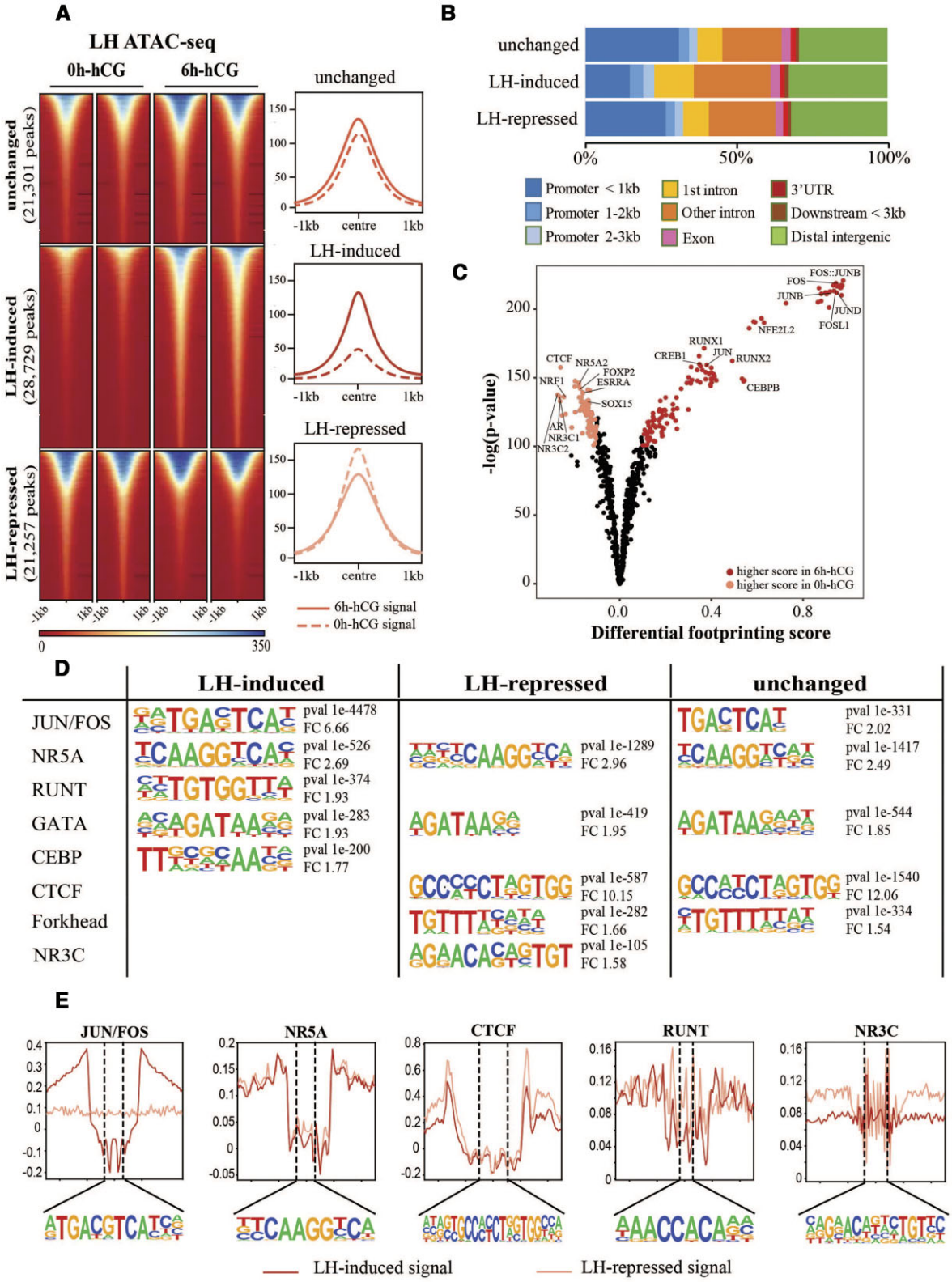

Figure 1. Global change in the chromatin landscape of granulosa cells after hCG treatment. (**A**) Heatmap of LH ATAC-peak signals (left), with peaks subset into those that were unchanged (top), LH-induced (middle) or LH-repressed (bottom). Representative profile plots of each condition are on the right. (**B**) Genomic distribution of ATAC-peaks that were unchanged by LH, LH-induced or LH-repressed. (**C**) Differential analysis of transcription factor-binding motifs in ATAC-seq peaks found in 6 h-hCG and 0 h-hCG. Top 5% motifs that were differentially enriched in either condition are highlighted. (**D**) *de novo* motif enrichment analysis of LH-induced, LH-repressed or unchanged ATAC peaks as identified through HOMER. For each dataset, top 5 motifs are shown with *P*-value and fold change to background (FC). (**E**) DNA footprints of selected motifs in ATAC-peaks that were LH-induced (red) or LH-repressed (pink). Footprinting score for each motif was calculated using the TOBIAS package as described in Methods, and shown across motif centre ±30 bp window with the core motif sequence within dashed lines.

scription factors, such as for JUN/FOS, RUNX, CREB and CEBPβ, showed significantly increased binding score in peaks for open chromatin after LH-stimulus, whereas those for CTCF, NR5A and ESRR were enriched at pre-LH open chromatin sites. Interestingly, the canonical motifs for the NR3C family, which includes PGR, glucocorticoid receptor (NR3C1/GR), mineralocorticoid receptor (NR3C2/MR) and androgen receptor (NR3C4/AR), showed significantly higher binding scores in open chromatin before LH-stimulus. In support of these findings, *de novo* motif enrichment analysis using HOMER also identified JUN/FOS, RUNT and CEBP motifs in LH-induced, but not LH-repressed open chromatin regions (Figure 1D). Motifs for NR5A and GATA families were similarly enriched in all ATAC-seq peak subsets. Importantly, a motif best matched to that bound by NR3C members was identified only in the LH-repressed subset, consistent with the differential transcription factor binding analysis pattern. Direct binding of transcription factors to these motifs was evident in aggregated footprint plots (Figure 1E). Footprint patterns indicative of transcription factors bound to these sites could be observed with medium to deep indentation (JUN/FOS, CTCF, NR5A) and shallower patterns (RUNT, NR3C), alluding to the differences in the dwell time of these transcription factors. Again JUN/FOS footprints were only evident after LH-stimulus, while evidence of NR3C footprints was most obvious in unstimulated cells.

Chromatin accessibility profiles were correlated with gene expression change in response to LH-stimulus through RNA-seq profiling of granulosa cells collected before or 8 h after *in vivo* LH-stimulus. A total of 2088 differentially expressed genes (DEG) were identified, of which 52% were upregulated by LH-stimulus (Figure 2A). This included many known genes associated with ovulation, such as *Ptgs2, Pgr, Runx1, Runx2* and *Adamts1* (Supplementary Table S2). Prediction of the potential upstream regulators of LH DEGs using Ingenuity Pathway Analysis (IPA) software identified a suite of transcription factors, many of which were also among the DEGs in response to the LH surge, including PGR (log FC = 6.4), RUNX1 (log FC = 4.6), CEBPβ (log FC = 2.5) and JUNB (log FC = 2.1) (Supplementary Tables S2 and S3). Notably, apart from PGR, the binding motifs for these same transcription factors also showed increased accessibility following LH-stimulus (Figure 1C, D). The global relationship between promoter accessibility and downstream gene expression in peri-ovulatory granulosa cells was demonstrated through a comparison between LH DEG and LH-dependent chromatin accessibility at the promoter (within 3 kb upstream of TSS) of these genes. Significant changes in promoter accessibility corresponded with transcriptional changes in 69.3% of LH-driven DEGs (1447 out of 2088 genes) (Figure 2B, red symbols). Promoter accessibility largely increased in LH-induced genes and was less accessible in LH-repressed genes (Spearman correlation coefficient = 0.4297). As examples, *Cxcr4* and *Inhbb*, two genes that were respectively upregulated and downregulated, show clear association between expression pattern and ATAC-seq signal at the gene promoter (Figure 2C). In some instances, however, genes that were differentially regulated had constitutively accessible promoters, as seen in *Cited1*. Transcriptionally active genes with LH-induced promoter accessibility were largely associated with biological processes that are important for ovulation, including angiogenesis, MAPK signalling pathway and inflammation response (Supplementary Figure S2). Altogether, these results showed that global chromatin remodelling in response to the LH surge, likely through the activation of a specific suite of transcription factors, drives the ovulatory gene expression profile that is important for LH-triggered ovulation.

PGR and RUNX1 mutually bind chromatin in peri-ovulatory granulosa cells

RUNX1 is functionally important in ovulation (51) and RUNT motifs are highly enriched in PGR ChIP-seq peaks in periovulatory granulosa cell (19). Furthermore, we found regions which gained chromatin accessibility after LH-stimulus contained enriched RUNT motifs (Figure 1C). Expression of RUNX1 and RUNX2 was induced in granulosa cells in response to the LH surge (Supplementary Figure S3A, B), and ovulation was delayed in granulosa cell-specific *Sf1*-cre RUNX1 KO mice (Supplementary Figure S3C). To determine whether RUNX1 is key to the transcriptional regulatory mechanism that mediates ovulatory gene expression, we used ChIP-seq to define genome-wide RUNX1 targets in granulosa cells before or 6 h after *in vivo* hCG treatment. Global RUNX1-chromatin binding was detected prior to the LH surge but was also induced 7-fold after the LH surge (16065 LH-induced peaks) (Figure 3A). LH-activated RUNX1 binding was strongly associated with LH-induced open chromatin as defined through ATAC-seq (Supplementary Figure S4A). A clear relationship between RUNX1 and PGR chromatin interaction in granulosa cells responding to LH stimulus was identified through comparative RUNX1 and PGR ChIP-seq. PGR and RUNX1 shared a remarkable number of mutual binding sites within 100 bp, with 9704 chromatin sites (70% of total PGR or 52% of total RUNX1 binding sites) having both PGR and RUNX1 binding (Figure 3B). Among these shared PGR/RUNX1 binding sites, 9288 were located in ATAC-seq open chromatin sites identified at the same time point. Subsetting transcriptionally active RUNX1 and PGR cistromes into those that were shared or uniquely-bound by each transcription factor shows PGR-bound sites without RUNX1 co-binding have a relatively low level of association with gene promoters. A strong preference for proximal promoter binding (within 1 kb of TSS) was a predominant characteristic of PGR/RUNX1 co-binding sites (Figure 3C). The remarkably high overlap of PGR and RUNX1 binding sites, coupled with our previous report of enriched RUNX1-binding motifs in granulosa cell PGR ChIP-seq (19) suggests that the previously reported granulosa-specific ability of PGR to target proximal promoter relies on co-binding with RUNX1. Such dependency was not reciprocal, as RUNX1 showed a prevalence for proximal promoter occupancy that was independent of PGR co-binding. To test whether LH-induced RUNX1 chromatin binding was dependent on PGR, we compared LH-induced RUNX1 binding intensity at PGR-overlapped sites versus PGR-independent sites. No difference was observed in the level of RUNX1 enrichment, suggesting that

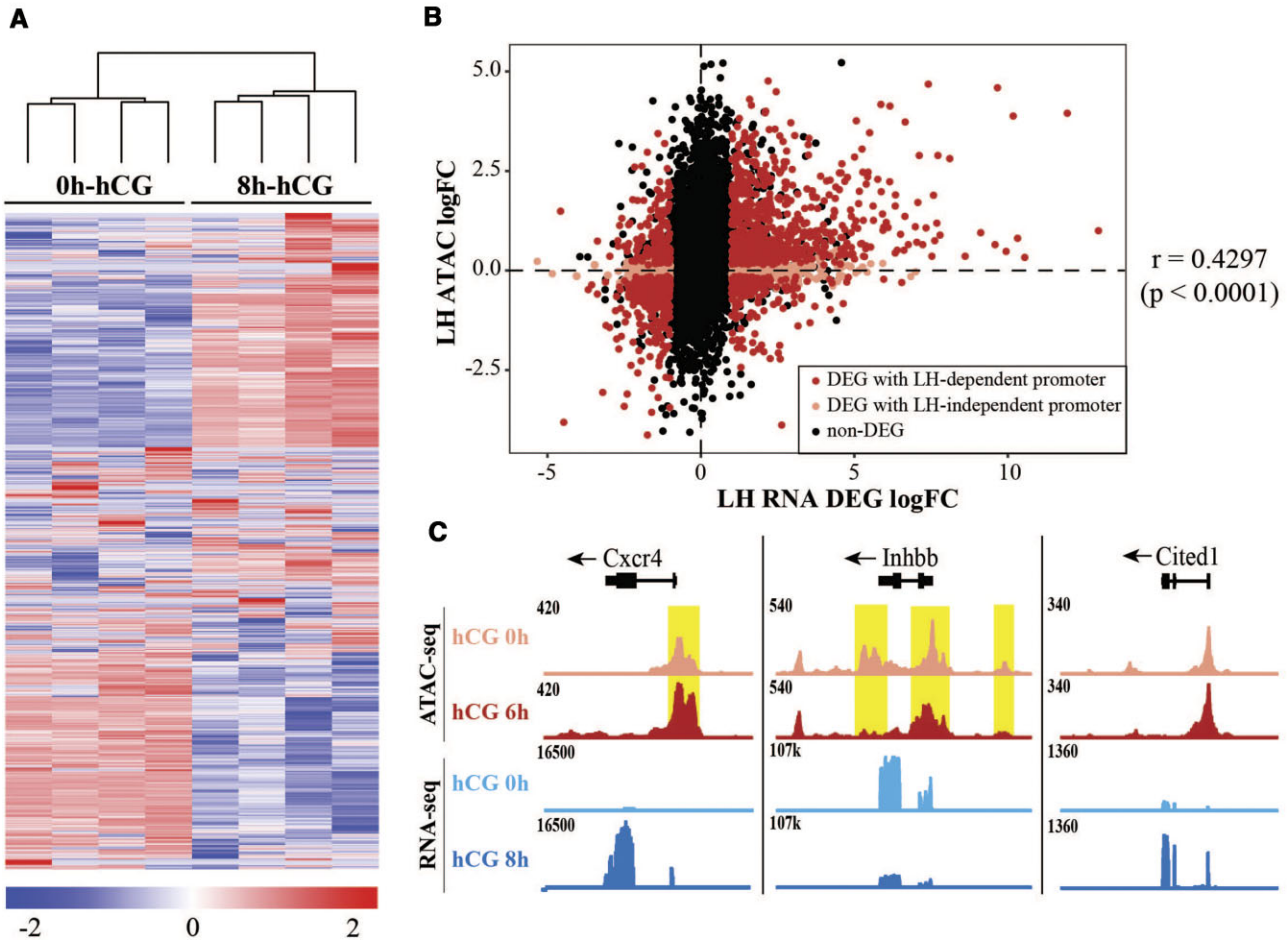

Figure 2. Global transcriptional change in granulosa cells after hCG treatment. (**A**) Heatmap of the expression level of ovulatory DEG identified in LH RNA-seq. Gene expression is shown as z-score calculated from log(CPM). (**B**) Correlation between expression level and promoter accessibility at RNA-seq identified ovulatory genes, shown as LH DEG RNA-seq log fold change versus ATAC-seq log fold change at their respective promoter (within 3 kb of TSS). DEGs with significant LH-dependent change in ATAC-seq signal in the promoter are labelled red, DEGs with non-significant change in promoter accessibility are labelled pink. Correlation between RNA-seq and ATAC-seq intensity is determined through Spearman's correlation coefficient ($r = 0.4297$, $P < 0.0001$). (**C**) Examples of ATAC-seq (tracks 1, 2) and RNA-seq (tracks 3, 4) signals for 0h-hCG (light) and 6h/8h-hCG (dark) at *Cxcr4, Inhbb* and *Cited1*. Differentially accessible ATAC peaks are highlighted in yellow.

PGR was unlikely to play a role in tethering or recruitment of RUNX1 to these shared sites (Supplementary Figure S4B).

The importance of PGR and RUNX1 cooperation on gene expression in response to the ovulatory signal at a genome-wide level was demonstrated by comparing genes with PGR and/or RUNX1 binding against our LH-responsive DEG list (Figure 3D). Remarkably, 62.4% of all LH-mediated DEGs contained at least PGR or RUNX1 binding at their proximal promoters (within 3 kb), with LH-induced DEGs more frequently bound by PGR and/or RUNX1 than LH-repressed DEGs (Supplementary Figure S4C). Of these, the majority of RUNX1- (55%) and PGR-bound (87%) LH DEGs were in fact co-bound by both transcription factors, implying that simultaneous interaction of both PGR and RUNX1 at target promoters is a major mechanism for each of these transcription factors in gene regulation. Examples of PGR/RUNX1 mutual chromatin occupancy were evident in the promoters of many known PGR and RUNX1 target genes in peri-ovulatory granulosa cells (*Rgcc* (52), *Adamts1* and *Cstl* (3)) (Figure 3E). PGR/RUNX1 cooperation may also regulate target genes via distal enhancers forming three-dimensional structures contacting the proximal promoters of regulated genes. To investigate this we integrated chromatin-chromatin interaction data from publicly-available mouse granulosa cell Hi-C (46). Hi-C identified distal chromatin interactions to the TSS of 516/2088 LH DEG, from which at least 28% were bound by PGR and/or RUNX1 (Figure 3D). Unlike PGR and RUNX1 binding at proximal promoters, PGR/RUNX1 binding at distal enhancers are equally associated with LH-induced and LH-repressed gene expression (Supplementary Figure S4C). An example for this distal regulation is seen in the PGR target gene *Adamts1*, which showed intense PGR/RUNX1 co-binding at distal regions interacting with the *Adamts1* TSS, indicated through Hi-C in mouse granulosa cells as well as promoter capture-C in human ovary (47) (Figure 3F).

Motif enrichment analysis showed that the expected canonical RUNT motif was highly and significantly en-

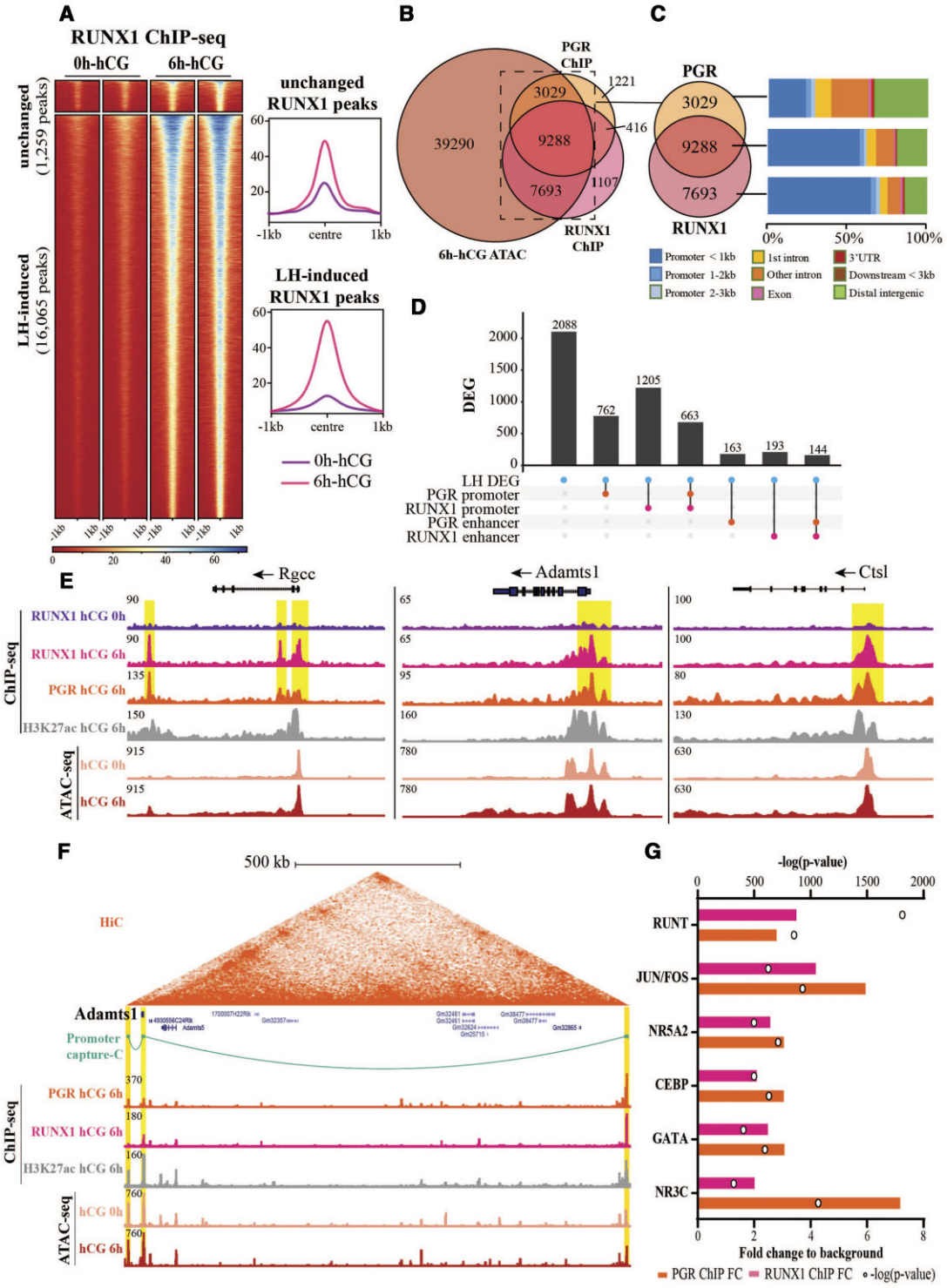

Figure 3. PGR and RUNX1 share mutual chromatin targets in peri-ovulatory granulosa cells. (**A**) Heatmap of RUNX1 ChIP-seq peak signals, with peaks subset into those that were unchanged (top) or LH-induced (bottom). Only 1 RUNX1 peak was LH-repressed and is thus not plotted. (**B**) Venn diagram showing shared and factor-unique peak counts for RUNX1 and PGR in relation to 6 h-hCG ATAC-seq peaks. (**C**) Genomic distribution of transcriptionally active PGR-specific (top), PGR/RUNX1 shared (middle) and RUNX1-specific (bottom) binding sites. (**D**) Upset plot showing the number of LH DEG with RUNX1 and/or PGR binding at their proximal promoters or enhancers. Promoter is defined as region ≤3 kb from TSS. Enhancer is defined as chromatin region interacting with TSS as identified through Hi-C (GSE154484). (**E**) Example of LH-dependent RUNX1 binding (tracks 1, 2) in conjunction with PGR (track 3) at *Rgcc*, *Adamts1* and *Cstl*. ATAC-seq peaks at 0, 6 h and H3K27ac ChIP-seq peaks at 6 h (tracks 4–6) indicate open chromatin regions. (**F**) Proximal and distal PGR/RUNX1 binding associated with PGR target gene *Adamts1*. From top to bottom: HiC at 10 kb bin (track 1), promoter capture-C (track 2), PGR & RUNX1 ChIP-seq (tracks 3, 4), LH ATAC-seq (tracks 5, 6), H3K27ac ChIP-seq (track 7). *Adamts1* TSS is highlighted in yellow and chromatin contacts are highlighted in orange. (**G**) Top most common known sequence motifs found to be enriched at RUNX1 (pink) and PGR (orange) binding sites. Bars indicate fold enrichment of motif to background (bottom *x*-axis). Circles indicate -log(p-value) (top *x*-axis).

riched in the RUNX1 cistrome (3.5-fold over background, *P*-value 1e–787) as well as PGR cistrome (2.8-fold, *P*-value 1e–370) (Figure 3G). The NR3C motif was also enriched in RUNX1-bound cistrome (2-fold over background, *P*-value 1e–25). This enrichment was restricted to only PGR/RUNX1 co-binding sites (Supplementary Figure S4D). Other enriched non-canonical motifs included those corresponding to JUN/FOS, CEBP and GATA transcription factors.

A close physical interaction between PGR and RUNX1 was supported by proximity ligation assay (PLA) of PGR/RUNX1 in the nucleus of mouse granulosa cells treated for up to 8 h with hCG and R5020 to mimic the *in vivo* ovulatory stimuli (Figure 4A). PLA signal showed a rapid transient induction of PGR/RUNX1 complexes by LH-stimulus, indicating an acute temporal PGR/RUNX1 interaction that was largely absent before stimulus but increased within 4 h of stimulation. Additionally, immunoprecipitation followed by mass spectrometry of PGR-binding protein partners in PGR-expressing human granulosa cells indicated the physical interaction between RUNX1 and PGR in response to R5020 treatment (Figure 4B). PGR can also interact with other RUNX members, as illustrated through PGR/RUNX2 PLA in granulosa cells exposed to ovulatory stimuli (Figure 4C).

PGR mediates chromatin accessibility in granulosa cells

PGR-bound regions predominantly overlap with transcriptionally active chromatin, as shown by 75% overlap in PGR- and H3K27ac ChIP-seq peaks (19) and 90% of PGR bound sites overlapping ATAC-seq peaks (Supplementary Figure S5A). In addition, an interaction between PGR and the histone acetyltransferase CBP/p300 was illustrated in hormone-stimulated granulosa cells (Supplementary Figure S5B). A functional relationship between PGR binding and chromatin accessibility was further investigated through ATAC-seq in granulosa cells of PGRWT and PGRKO mice. 1499 sites were found to have significantly altered peak intensity in the absence of PGR (Figure 5A); interestingly, only 6 of the 1499 sites had increased ATAC peak intensity in PGRKO compared to PGRWT while the majority of sites lost accessibility in PGRKO. Whereas PGR-chromatin binding favours proximal promoter regions in granulosa cells, the PGR-dependent ATAC-seq peaks were more evenly distributed throughout all genomic features (Figure 5B). The ablation of PGR resulted in the dysregulation of 236 genes, as identified through RNA-seq of PGRWT and PGRKO granulosa cells (Supplementary Table S2). Consistently a reduction in ATAC-seq intensity was evident at promoters of these PGR-dependent genes (Spearman correlation coefficient = 0.5116, *P*-value < 0.0001) (Figure 5C). This indicated that promoter accessibility for these genes is significantly influenced by PGR ablation. Examples of PGR-dependent chromatin accessibility are shown for *Gpt2*, whose promoter was differentially accessible in PGRKO, and *Abhd2*, the promoter accessibility of which was not significantly altered in the absence of PGR (Figure 5D).

Transcription factor motif enrichment analysis was performed on PGR-driven ATAC peaks and compared with motifs enriched in PGR ChIP-seq. As with ChIP-seq, the most highly enriched and most significant motif identified in PGR-driven ATAC peak sequences was the canonical NR3C motif (12.4-fold over background). Again as with PGR ChIP-seq, several non-canonical motifs were also significantly enriched in PGR-dependent ATAC-peaks (Figure 5E). Interestingly, 53% (795 of 1499) of PGR-dependent ATAC sites were bound by PGR, while only 17.8% (267 sites) showed any RUNX1 binding, almost all of which (250/267 sites) was bound by both PGR and RUNX1 (Figure 5F). Additionally, PGRKO ATAC-seq suggests that PGR directly promotes chromatin accessibility at a subset of regions through binding the canonical NR3C motif. To examine this we generated a quantitative model of NR3C DNA binding using closely related AR HT-SELEX data (41,42). Energy logos (15 bp) derived from dinucleotide models of DNA-binding conformed to the NR3C consensus or PGR motif (Supplementary Figure S6A). Next, we used this model to estimate PGR binding affinity within each peak and compared this to PGR ChIP-seq peak intensity, which showed a modest linear relationship to PGR binding scores (Supplementary Figure S6B). We examined the ability of DNA binding models to predict PGR chromatin occupation by Receiver Operator Characteristic (ROC) curve analysis and found that binding affinity predicted chromatin occupancy only modestly for all PGR ChIP sites (AUROC = 0.63, n = 13 976) but highly accurately at PGR ChIP peaks that were also PGR-dependent ATAC-seq peaks (AUROC = 0.9, n = 804) (Figure 5G). This was supported by significantly stronger ChIP peak intensity and NR3C motif binding affinities (Figure 5H) at PGR-bound PGR-dependent ATAC peaks compared to all PGR binding sites. Taken together, this suggests that PGR drives chromatin remodelling through binding NR3C motifs at select chromatin regions, while shared PGR/RUNX binding at non-canonical sites are less dependent on PGR for promoting chromatin accessibility.

PGR isoforms mediate specific ovulatory gene regulation

The disrupted ovulatory phenotype has previously been documented in both total PGRKO and AKO mice but not BKO mice (20,21), which we verified through ovulation rate assessment on these three mouse strains (Supplementary Figure S7). We performed RNA-seq in granulosa cells obtained from PGRKO, AKO or BKO and WT littermates from each strain, and hierarchical clustering showed that the global gene expression pattern in AKO granulosa cells resembled that of total PGRKO, while BKO more closely resembled the WTs of each strain (Figure 6A). Differential expression of 310 genes was identified in AKO, 153 (or 49.4%) of which were also identified in the absence of both PGR isoforms (Figure 6B, Supplementary Table S2). Among these, 48.6% and 58.5% of AKO and PGRKO DEG respectively were also differentially expressed in response to the LH surge. The loss of PGR-B, on the other hand, resulted in no significant transcriptional changes (Figure 6B).

To identify transcription factors that co-regulate downstream PGR target genes, upstream regulators of the DEG datasets were analyzed using IPA (Figure 6C). As expected, PGR was shown to be the most significant reg-

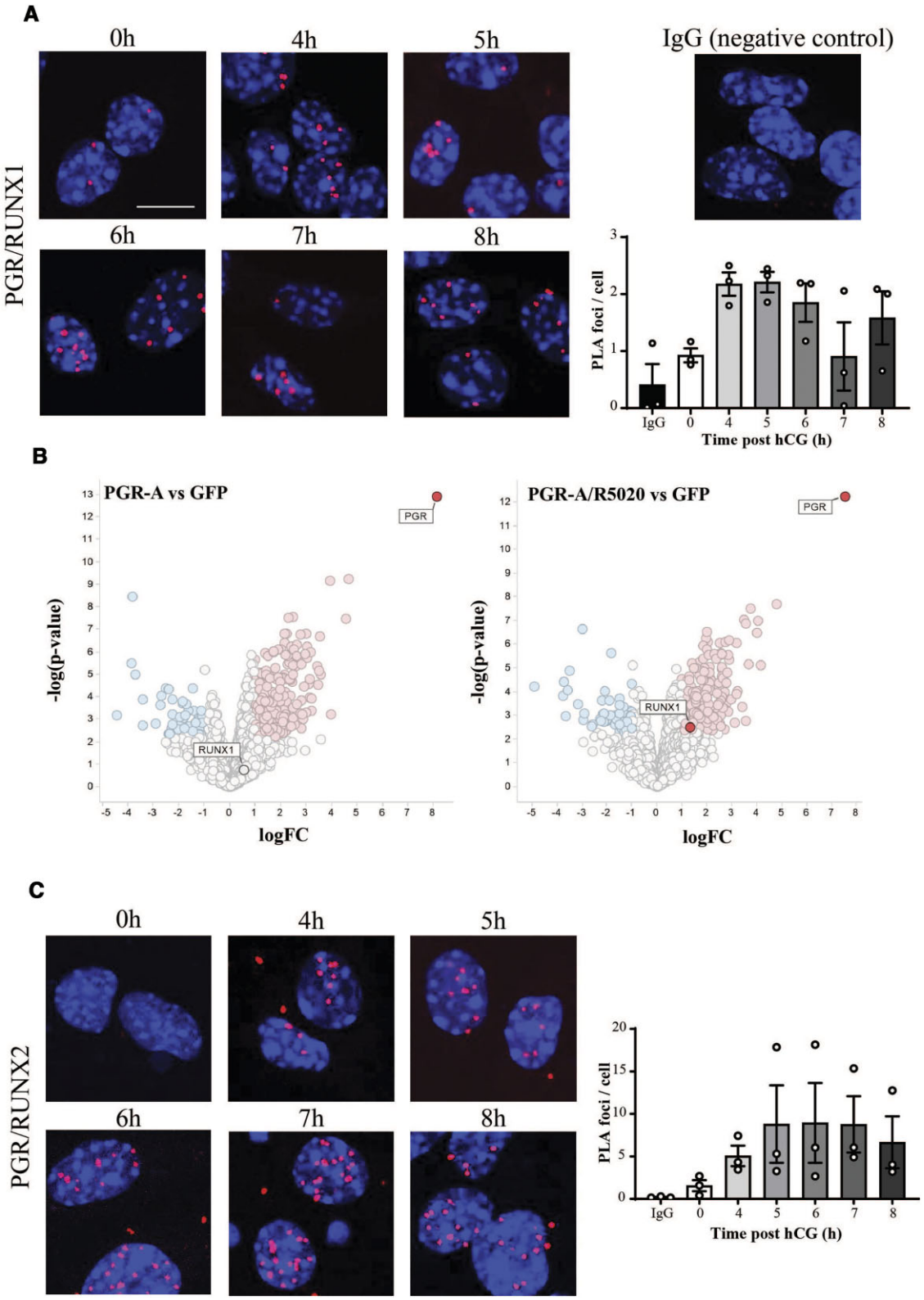

Figure 4. PGR interacts with RUNX transcription factors in granulosa cells in response to the LH surge. PLA for PGR/RUNX1. (**A**) and PGR/RUNX2 (**C**) in cultured granulosa cells under hCG/R5020 time course treatment. One representative image is shown for each treatment. PGR/IgG antibody pair was used as negative control. PLA was performed in three biological replicates (4 mice per replicate). Quantification of PLA signal is displayed as the number of nuclear foci per cell, displayed as mean ± SEM, *P*-value = 0.1044 (A), *P*-value = 0.2294 (**C**). Red indicates protein-protein interaction. Blue is DAPI nuclear stain. Scale bar = 10 μm. (**B**) PGR-A interacting proteins in PGR-A overexpressed KGN cells detected using immunoprecipitation-mass spectrometry, shown in comparison to GFP control. Volcano plots are shown for proteins detected without (left) or with (right) R5020 treatment for 4 h, with RUNX1 highlighted. Colored dots indicate statistical significance (log(*P*-adjusted) ≤ 0.05, log(fold change) ≥ 1), high in PGR-A (red) or high in GFP (blue). $n = 5$ per group.

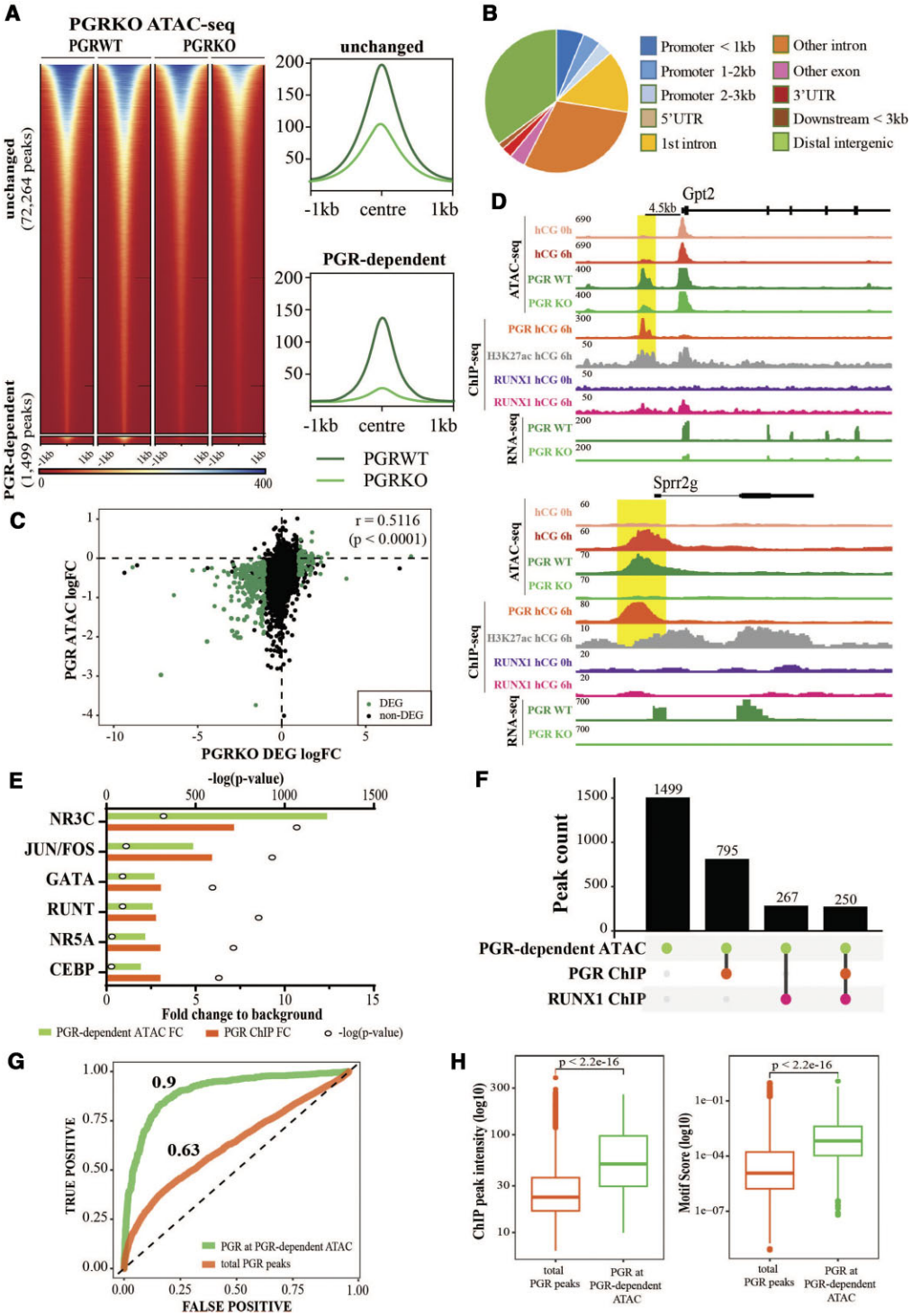

Figure 5. PGR mediates chromatin accessibility in granulosa cells. (**A**) Heatmap of PGR ATAC-peaks (left) that were unchanged (top) or differentially accessible between PGRKO WT and KO (bottom). Representative profile plots of each group are on the right. (**B**) Genomic distribution of PGR-dependent ATAC-seq peaks. (**C**) Correlation between expression level and promoter accessibility at PGR DEGs, shown as PGR DEG fold change versus ATAC fold change at their respective promoter. DEGs with PGR-dependent promoter accessibility are labelled green. Light green depicts statistically significant PGR-dependent change in promoter accessibility. Correlation between RNA-seq and ATAC-seq intensity is determined through Spearman's correlation coefficient ($r = 0.5116$, $P < 0.0001$). (**D**) Examples of LH ATAC-seq (tracks 1, 2), PGR ATAC-seq (tracks 3, 4), PGR and H3K27ac ChIP-seq (tracks 5, 6) and PGR RNA-seq (tracks 7, 8) signals at *Gpt2* and *Abhd2*. ATAC peaks at promoters are highlighted in yellow. (**E**) Top most common known sequence motifs found to be enriched at PGR-dependent ATAC peaks (green), with the level of enrichment for the same motif at PGR bound ChIP-seq sites (orange). Bars indicate fold enrichment of motif to background (bottom x axis). Circles indicate –log(*P*-value) (top *x*-axis). (**F**) Upset plot showing the number of overlapped peaks between PGR-dependent ATAC sites, PGR and RUNX1 bound ChIP-seq sites. (**G**) ROC curves of PGR binding prediction using NR3C dinucleotide model at total PGR peaks (orange) and PGR binding at PGR-dependent ATAC sites (green). (**H**) PGR ChIP-seq peak intensity (left) and NR3C motif score (right) of total PGR peaks and PGR binding at PGR-dependent ATAC sites.

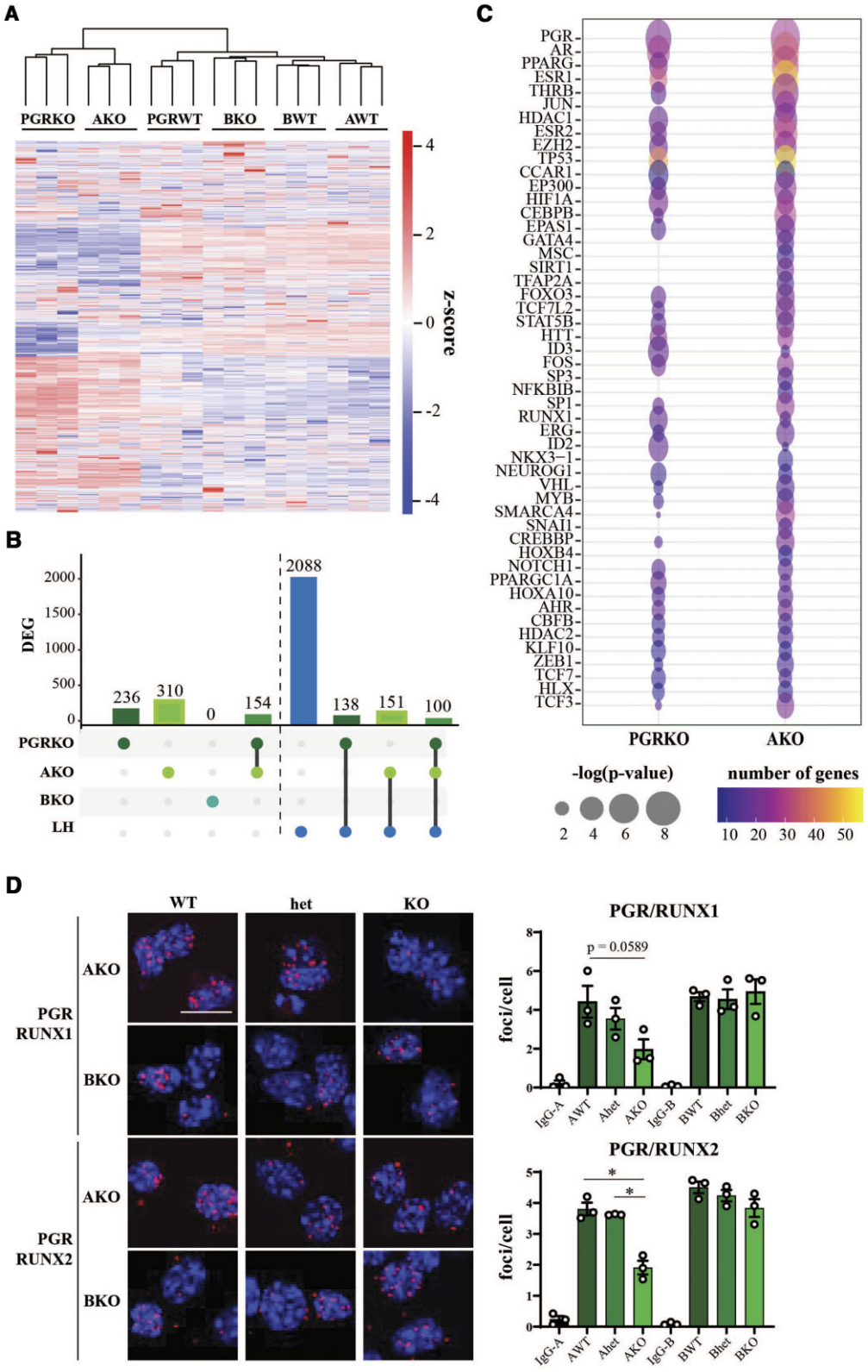

Figure 6. PGR isoform-driven transcriptome in peri-ovulatory granulosa cells through interaction with specific transcription factor partners. (**A**) Heatmap showing changes in gene expression in granulosa cells that are WT or KO for total PGR, PGR-A or PGR-B, each shown with the collective PGRKO, AKO and BKO DEGs. Gene expression is shown as *z*-score calculated from log(CPM). (**B**) Upset plot showing the number of overlapped genes between PGRKO/AKO/BKO DEG and LH DEG. (**C**) Top 50 upstream regulators of PGRKO and AKO DEGs as identified through IPA. Circle colour indicates the number of downstream DEG regulated by the upstream regulator, circle size indicates -log(p-value) of regulator enrichment. (**D**) PLA of PGR/RUNX1 (top) and PGR/RUNX2 (bottom) in *in vitro* WT/het/KO granulosa cells from AKO or BKO mice, treated for 6 h with hCG and R5020. Red indicates protein-protein interaction. Blue is DAPI nuclear stain. Scale bar = 10 μm. Quantification of PLA signal is displayed as the number of nuclear foci per cell, displayed as mean ± SEM, * *P*-value < 0.05, *N* = 3 biological replicates (two mice per replicate per genotype).

ulator in both PGRKO and AKO datasets. Additionally, transcription factors that are known to be induced by PGR, such as PPARG (53) and HIF1A (54) were also enriched in both datasets. Importantly, this independent approach also supports RUNX, JUN/FOS and CBP/p300 as mediators of the PGR-dependent transcriptional response (19), as RUNX1, CBFβ, JUN, FOS and p300 were also identified through upstream analysis. We performed PLA for PGR/RUNX1 and PGR/RUNX2 in hCG/progestin-stimulated granulosa cells obtained from WT, het and KO animals from the AKO and BKO strains. A decrease in protein-protein interaction with both RUNX1 and RUNX2 was observed in AKO but not BKO granulosa cells (Figure 6D).

DISCUSSION

Our characterization of transcriptome and chromatin remodelling in granulosa cells responding to *in vivo* ovulatory stimulus has identified an ovary-specific gene regulatory network involving the interaction of PGR and RUNX. The results indicate two modes of action for PGR—co-binding of PGR and RUNX at non-canonical DNA motifs, and NR3C motif-driven PGR binding and chromatin remodelling—through which PGR modulates chromatin and transcriptional profiles.

The LH-surge induces extensive changes in the chromatin landscape and the ovarian gene expression profile, resulting in the activation of biological processes required for follicle rupture as well as luteinization. Extensive chromatin remodelling within 6 h of the ovulatory stimulus is an example of rapid, pervasive hormonal reprogramming of gene expression *in vivo*. ATAC-seq with *de novo* motif identification and footprinting analysis confirmed RUNX, JUN/FOS, NR5A and CEBP transcription factor binding mediate LH-dependent chromatin opening. This is consistent with the reported induced expression of JUN and FOS (55), RUNX1/2 (56,57), LRH1 (58) and CEBPβ (59) by ovulatory stimulus (60,61).

PGR and RUNX co-binding at promoters is a key feature of ovulatory genes. A remarkable overlap in PGR/RUNX1 occupancy, accounting for 70% of total PGR binding sites, is particularly abundant at TSS of ovulatory genes. This was further supported by PLA and immunoprecipitation-mass spectrometry, which demonstrate a close physical association of PGR and RUNX1 in granulosa cell that was specifically induced in the presence of PGR agonist. Enriched PGR-promoter binding was dependent on RUNX1, while preferential RUNX1 binding to proximal promoters was independent of PGR. Genes whose proximal promoter was co-occupied by both PGR and RUNX1 include well-described downstream target genes of PGR (*Adamts1, Cstl* (3)) as well as RUNX1 target gene (*Rgcc*) (52), which are involved in extracellular matrix remodelling and cell cycle regulation, respectively. In addition to co-binding at promoter regions, PGR/RUNX1 interaction is also evident at enhancers that are distal to target genes, shown through chromatin looping that establishes contacts between shared PGR/RUNX1 sites and TSS of ovulatory genes including *Adamts1*. The conclusion that RUNX guides PGR binding to granulosa-specific chromatin targets is supported by the reported interactions between RUNX and close NR3C family members, AR and GR, (62–65), as well as RUNX1 tethering of ERα-chromatin binding (66). Thus PGR/RUNX1 interaction guides PGR binding to promoter regions to cooperatively regulate the ovulatory gene expression program. While PGR/RUNX interaction is crucial for PGR ovulatory action, disruptions in RUNX action are not sufficient to completely block ovulation. RUNX1 by itself is not obligatory for ovulation, since granulosa-specific ablation of RUNX1 caused only a minor delay in ovulation and no fertility defect. Blocking the action of both RUNX1 and RUNX2 through the ablation of their shared co-factor CBFβ caused 70% reduction in ovulation rate (67).

Our present genomic results, together with the reported ovulatory defects in knockout mouse models, support a functional interaction between PGR and RUNX1/2 in ovulation. Showing that depletion of RUNX1 and RUNX2 disrupts PGR target gene expression would be definitive proof of this model; however, embryonic lethality of RUNX1/2 null mice and the roles of RUNX1/2 in granulosa cell specification (51,68) confound these experiments. In addition to RUNX interaction, other mechanisms are also involved in PGR ovulatory actions. Other proposed co-regulators of PGR in granulosa cells include transcription factors belonging to the JUN/FOS and CEBP family, both of which are also activated in granulosa cells in response to the LH surge. JUN/FOS transcription factors are involved in prostaglandin production and metabolism in granulosa cells (69,70), while the ablation of both CEBPα and CEBPβ results in complete anovulation and luteinization defects in mice (59). Whether these transcription factors also cooperate with PGR to exert ovulatory roles will require further investigation.

Surprisingly, chromatin sites with the canonical motif bound by NR3C steroid receptors including PGR was more highly occupied prior to the LH-surge, in spite of the very large LH induction of PGR. While this does not discount the involvement of the canonical PGR mechanism via NR3C motif binding in the ovarian context, it is an indication that in granulosa cells, NR3C motif-independent PGR action is more prevalent, a likely model of which is the PGR/RUNX1 cooperation described above. Despite this, a subset of post-LH open chromatin regions was found to be PGR-dependent, since deletion of PGR caused loss of accessibility in these regions. These regions also showed significantly higher binding affinity for the canonical NR3C motif and significantly higher PGR ChIP-seq peak intensity, with no preference for gene promoters. The lack of PGR/RUNX1 co-binding at PGR-dependent ATAC sites indicates that PGR-driven chromatin opening is not dependent on PGR/RUNX interaction. Instead, direct PGR binding to the full palindromic NR3C DNA motif is key to PGR-mediated chromatin accessibility, indicating that PGR itself can act as a pioneer factor that enables structural modification and activation of chromatin, likely involving the recruitment of the histone acetyltransferase CBP/p300 by PGR, as shown through PLA. While the contribution of NR3C canonical mechanism is highly selective in PGR action in granulosa cells, the high level of NR3C motif enrichment at pre-LH accessible chromatin suggests that this

remains a highly-utilized mechanisms for other NR3C transcription factors that are more active prior to the LH-surge. In particular, AR is expressed in granulosa cells at various stages of follicle development and has important roles in folliculogenesis, including promoting granulosa cell proliferation and preventing atresia (71). The direct role of AR in ovulation is less clear; however, AR mRNA expression is reduced in granulosa cells following LH-stimulus (72,73), which might explain the net loss of NR3C enrichment in post-LH chromatin.

Together the results suggest that the tissue-specific ovulatory response in granulosa cells is driven by proximal promoter PGR/RUNX interaction as well as RUNX1-independent PGR binding outside of proximal regions that facilitates new chromatin accessibility. Transcriptional induction of specific target genes may also involve tertiary chromatin structure bringing distal enhancer regions and gene TSSs into contact. Our results refine the mechanistic model of PGR action in granulosa cells and such ovarian-specific molecular mechanism of PGR action is distinct from the mechanisms in other PGR-responsive organs (9,19). These insights are critical for understanding and addressing causes of anovulatory infertility and for the development of specific ovulation-targeting contraceptives.

DATA AVAILABILITY

The datasets generated and/or analyzed during the current study are available in the NCBI Gene Expression Omnibus repository: GSE166878 (LH and PGRKO ATAC-seq), GSE178314 (LH RNA-seq – token ghabquauhxkljcp), GSE168213 (PGRKO RNA-seq), GSE152941 (RUNX1 ChIP-seq). Previously published data accessed at GSE86189 (human ovary promoter capture-C), GSE154484 (mouse granulosa cell Hi-C).

SUPPLEMENTARY DATA

Supplementary Data are available at NAR Online.

ACKNOWLEDGEMENTS

The RUNX1 antibody for ChIP-seq was a kind gift from Dr Yoram Groner and Dr Ditsa Levanon, the Weizmann Institute of Science, Israel.

FUNDING

Bill and Melinda Gates Foundation Contraceptive Discovery Program [OPP1171844, INV-001616]; D.L.R. is supported by NHMRC Senior Research Fellowship [APP1110562]; R.L.R. is supported by NHMRC Senior Research Fellowship [APP1117976]; Intramural Research Program of National Institute of Environmental Health Sciences in the USA [Z01-ES102965] for HHCY. Funding for open access charge: Bill and Melinda Gates Foundation Contraceptive Discovery Program (OPP1171844, INV-001616).

Conflict of interest statement. None declared.

REFERENCES

1. Russell,D.L. and Robker,R.L. (2019) In Leung,P.C.K. and Adashi,E.Y. (eds.) *The Ovary. 3rd edn*. Academic Press, pp. 217–234.
2. Hughes,C.H.K. and Murphy,B.D. (2021) Nuclear receptors: key regulators of somatic cell functions in the ovulatory process. *Mol. Aspects Med.*, **78**, 100937.
3. Robker,R.L., Russell,D.L., Espey,L.L., Lydon,J.P., O'Malley,B.W. and Richards,J.S. (2000) Progesterone-regulated genes in the ovulation process: ADAMTS-1 and cathepsin L proteases. *Proc. Natl. Acad. Sci. U.S.A.*, **97**, 4689–4694.
4. Park,C.J., Lin,P.-C., Zhou,S., Barakat,R., Bashir,S.T., Choi,J.M., Cacioppo,J.A., Oakley,O.R., Duffy,D.M., Lydon,J.P. *et al.* (2020) Progesterone receptor serves the ovary as a trigger of ovulation and a terminator of inflammation. *Cell Rep.*, **31**, 107496.
5. McNatty,K.P., Makris,A., De Grazia,C., Osathanondh,R. and Ryan,K.J. (1979) The production of progesterone, androgens and oestrogens by human granulosa cells in vitro and in vivo. *J. Steroid Biochem.*, **11**, 775–779.
6. Lydon,J.P., DeMayo,F.J., Funk,C.R., Mani,S.K., Hughes,A.R., Montgomery,C.A. Jr., Shyamala,G., Conneely,O.M. and O'Malley,B.W. (1995) Mice lacking progesterone receptor exhibit pleiotropic reproductive abnormalities. *Genes Dev.*, **9**, 2266–2278.
7. Ledger,W.L., Sweeting,V.M., Hillier,H. and Baird,D.T. (1992) Inhibition of ovulation by low-dose mifepristone (RU 486). *Hum. Reprod.*, **7**, 945–950.
8. Brache,V., Cochon,L., Jesam,C., Maldonado,R., Salvatierra,A.M., Levy,D.P., Gainer,E. and Croxatto,H.B. (2010) Immediate pre-ovulatory administration of 30 mg ulipristal acetate significantly delays follicular rupture. *Hum. Reprod.*, **25**, 2256–2263.
9. Yin,P., Roqueiro,D., Huang,L., Owen,J.K., Xie,A., Navarro,A., Monsivais,D., Coon V,J.S., Kim,J.J., Dai,Y. *et al.* (2012) Genome-wide progesterone receptor binding: cell type-specific and shared mechanisms in T47D breast cancer cells and primary leiomyoma cells. *PLoS One*, **7**, e29021.
10. Li,X. and O'Malley,B.W. (2003) Unfolding the action of progesterone receptors. *J. Biol. Chem.*, **278**, 39261–39264.
11. Han,S.J., DeMayo,F.J., Xu,J., Tsai,S.Y., Tsai,M.-J. and O'Malley,B.W. (2006) Steroid receptor coactivator (SRC)-1 and SRC-3 differentially modulate tissue-specific activation functions of the progesterone receptor. *Mol. Endocrinol.*, **20**, 45–55.
12. Béguelin,W., Díaz Flaqué,M.C., Proietti,C.J., Cayrol,F., Rivas,M.A., Tkach,M., Rosemblit,C., Tocci,J.M., Charreau,E.H., Schillaci,R. *et al.* (2010) Progesterone receptor induces ErbB-2 nuclear translocation to promote breast cancer growth via a novel transcriptional effect: erbB-2 function as a coactivator of Stat3. *Mol. Cell. Biol.*, **30**, 5456–5472.
13. Malbeteau,L., Poulard,C., Languilaire,C., Mikaelian,I., Flamant,F., Le Romancer,M. and Corbo,L. (2020) PRMT1 is critical for the transcriptional activity and the stability of the progesterone receptor. *Iscience*, **23**, 101236.
14. Cho,H., Orphanides,G., Sun,X., Yang,X.J., Ogryzko,V., Lees,E., Nakatani,Y. and Reinberg,D. (1998) A human RNA polymerase II complex containing factors that modify chromatin structure. *Mol. Cell. Biol.*, **18**, 5355–5363.
15. Dong,X., Challis,J.R. and Lye,S.J. (2004) Intramolecular interactions between the AF3 domain and the C-terminus of the human progesterone receptor are mediated through two LXXLL motifs. *J. Mol. Endocrinol.*, **32**, 843–857.
16. Merlino,A.A., Welsh,T.N., Tan,H., Yi,L.J., Cannon,V., Mercer,B.M. and Mesiano,S. (2007) Nuclear progesterone receptors in the human pregnancy Myometrium: evidence that parturition involves functional progesterone withdrawal mediated by increased expression of progesterone receptor-A. *J. Clin. Endocrinol. Metab.*, **92**, 1927–1933.
17. Menendez,J.A., Peirce,S.K., Papadimitropoulou,A., Cuyàs,E., Steen,T.V., Verdura,S., Vellon,L., Chen,W.Y. and Lupu,R. (2020) Progesterone receptor isoform-dependent cross-talk between prolactin and fatty acid synthase in breast cancer. *Aging (Albany NY)*, **12**, 24671–24692.
18. Teilmann,S.C., Clement,C.A., Thorup,J., Byskov,A.G. and Christensen,S.T. (2006) Expression and localization of the progesterone receptor in mouse and human reproductive organs. *J. Endocrinol.*, **191**, 525–535.

19. Dinh,D.T., Breen,J., Akison,L.K., DeMayo,F.J., Brown,H.M., Robker,R.L. and Russell,D.L. (2019) Tissue-specific progesterone receptor-chromatin binding and the regulation of progesterone-dependent gene expression. *Sci. Rep.*, **9**, 11966–11966.
20. Mulac-Jericevic,B., Mullinax,R.A., DeMayo,F.J., Lydon,J.P. and Conneely,O.M. (2000) Subgroup of reproductive functions of progesterone mediated by progesterone receptor-B isoform. *Science*, **289**, 1751–1754.
21. Mulac-Jericevic,B., Lydon,J.P., DeMayo,F.J. and Conneely,O.M. (2003) Defective mammary gland morphogenesis in mice lacking the progesterone receptor B isoform. *Proc. Natl. Acad. Sci. U.S.A.*, **100**, 9744–9749.
22. Hu,M., Li,J., Zhang,Y., Li,X., Brännström,M., Shao,L.R. and Billig,H. (2018) Endometrial progesterone receptor isoforms in women with polycystic ovary syndrome. *Am. J. Transl. Res.*, **10**, 2696–2705.
23. Wetendorf,M., Li,R., Wu,S.-P., Liu,J., Creighton,C.J., Wang,T., Janardhan,K.S., Willson,C.J., Lanz,R.B., Murphy,B.D. *et al.* (2020) Constitutive expression of progesterone receptor isoforms promotes the development of hormone-dependent ovarian neoplasms. *Sci. Signal*, **13**, eaaz9646.
24. Wu,S.-P., Li,R. and DeMayo,F.J. (2018) Progesterone Receptor Regulation of Uterine Adaptation for Pregnancy. *Trends Endocrinol. Metab.*, **29**, 481–491.
25. Corces,M.R., Trevino,A.E., Hamilton,E.G., Greenside,P.G., Sinnott-Armstrong,N.A., Vesuna,S., Satpathy,A.T., Rubin,A.J., Montine,K.S., Wu,B. *et al.* (2017) An improved ATAC-seq protocol reduces background and enables interrogation of frozen tissues. *Nat. Methods*, **14**, 959–962.
26. Martin,M. (2011) Cutadapt removes adapter sequences from high-throughput sequencing reads. *EMBnet. J.*, **17**, 10–12.
27. Langmead,B. and Salzberg,S.L. (2012) Fast gapped-read alignment with Bowtie 2. *Nat. Methods*, **9**, 357–359.
28. Zhang,Y., Liu,T., Meyer,C.A., Eeckhoute,J., Johnson,D.S., Bernstein,B.E., Nusbaum,C., Myers,R.M., Brown,M., Li,W. *et al.* (2008) Model-based analysis of ChIP-Seq (MACS). *Genome Biol.*, **9**, R137.
29. Stark,R. and Brown,G. (2011) *DiffBind: differential binding analysis of ChIP-Seq peak data*. https://bioconductor.org/packages/devel/bioc/vignettes/DiffBind/inst/doc/DiffBind.pdf.
30. Ramírez,F., Ryan,D.P., Grüning,B., Bhardwaj,V., Kilpert,F., Richter,A.S., Heyne,S., Dündar,F. and Manke,T. (2016) deepTools2: a next generation web server for deep-sequencing data analysis. *Nucleic Acids Res.*, **44**, W160–W165.
31. Yu,G., Wang,L.G. and He,Q.Y. (2015) ChIPseeker: an R/Bioconductor package for ChIP peak annotation, comparison and visualization. *Bioinformatics*, **31**, 2382–2383.
32. McLean,C.Y., Bristor,D., Hiller,M., Clarke,S.L., Schaar,B.T., Lowe,C.B., Wenger,A.M. and Bejerano,G. (2010) GREAT improves functional interpretation of cis-regulatory regions. *Nat. Biotechnol.*, **28**, 495.
33. Bentsen,M., Goymann,P., Schultheis,H., Klee,K., Petrova,A., Wiegandt,R., Fust,A., Preussner,J., Kuenne,C., Braun,T. *et al.* (2020) ATAC-seq footprinting unravels kinetics of transcription factor binding during zygotic genome activation. *Nat. Commun.*, **11**, 4267.
34. Heinz,S., Benner,C., Spann,N., Bertolino,E., Lin,Y.C., Laslo,P., Cheng,J.X., Murre,C., Singh,H. and Glass,C.K. (2010) Simple combinations of lineage-determining transcription factors prime cis-regulatory elements required for macrophage and B cell identities. *Mol. Cell*, **38**, 576–589.
35. Lindgreen,S. (2012) AdapterRemoval: easy cleaning of next-generation sequencing reads. *BMC Research Notes*, **5**, 337.
36. Patro,R., Duggal,G., Love,M.I., Irizarry,R.A. and Kingsford,C. (2017) Salmon provides fast and bias-aware quantification of transcript expression. *Nat. Methods*, **14**, 417.
37. Ritchie,M.E., Phipson,B., Wu,D., Hu,Y., Law,C.W., Shi,W. and Smyth,G.K. (2015) limma powers differential expression analyses for RNA-sequencing and microarray studies. *Nucleic Acids Res.*, **43**, e47.
38. Robinson,M.D., McCarthy,D.J. and Smyth,G.K. (2010) edgeR: a Bioconductor package for differential expression analysis of digital gene expression data. *Bioinformatics*, **26**, 139–140.
39. Umansky,K.B., Gruenbaum-Cohen,Y., Tsoory,M., Feldmesser,E., Goldenberg,D., Brenner,O. and Groner,Y. (2015) Runx1 transcription factor is required for myoblasts proliferation during muscle regeneration. *PLos Genet.*, **11**, e1005457.
40. Zhu,L.J., Gazin,C., Lawson,N.D., Pagès,H., Lin,S.M., Lapointe,D.S. and Green,M.R. (2010) ChIPpeakAnno: a Bioconductor package to annotate ChIP-seq and ChIP-chip data. *BMC Bioinf.*, **11**, 237.
41. Jolma,A., Yan,J., Whitington,T., Toivonen,J., Nitta,K.R., Rastas,P., Morgunova,E., Enge,M., Taipale,M., Wei,G. *et al.* (2013) DNA-binding specificities of human transcription factors. *Cell*, **152**, 327–339.
42. Yang,L., Orenstein,Y., Jolma,A., Yin,Y., Taipale,J., Shamir,R. and Rohs,R. (2017) Transcription factor family-specific DNA shape readout revealed by quantitative specificity models. *Mol. Syst. Biol.*, **13**, 910.
43. Rastogi,C., Rube,H.T., Kribelbauer,J.F., Crocker,J., Loker,R.E., Martini,G.D., Laptenko,O., Freed-Pastor,W.A., Prives,C., Stern,D.L. *et al.* (2018) Accurate and sensitive quantification of protein-DNA binding affinity. *Proc. Natl. Acad. Sci. U.S.A.*, **115**, E3692–E3701.
44. Bersten,D., Sullivan,A., McDougal,D., Breen,J., Fitzsimmons,R., Muscat,G., Pederson,S., Bruning,J., Fan,C., Thomas,P. *et al.* (2022) Core and Flanking bHLH-PAS:DNA interactions mediate specificity and drive obesity. bioRxiv doi: https://doi.org/10.1101/2022.02.01.475276, 02 February 2022, preprint: not peer reviewed.
45. Robin,X., Turck,N., Hainard,A., Tiberti,N., Lisacek,F., Sanchez,J.-C. and Müller,M. (2011) pROC: an open-source package for R and S+ to analyze and compare ROC curves. *BMC Bioinf.*, **12**, 77.
46. Lindeman,R.E., Murphy,M.W., Agrimson,K.S., Gewiss,R.L., Bardwell,V.J., Gearhart,M.D. and Zarkower,D. (2021) The conserved sex regulator DMRT1 recruits SOX9 in sexual cell fate reprogramming. *Nucleic Acids Res.*, **49**, 6144–6164.
47. Jung,I., Schmitt,A., Diao,Y., Lee,A.J., Liu,T., Yang,D., Tan,C., Eom,J., Chan,M., Chee,S. *et al.* (2019) A compendium of promoter-centered long-range chromatin interactions in the human genome. *Nat. Genet.*, **51**, 1442–1449.
48. Ramírez,F., Bhardwaj,V., Arrigoni,L., Lam,K.C., Grüning,B.A., Villaveces,J., Habermann,B., Akhtar,A. and Manke,T. (2018) High-resolution TADs reveal DNA sequences underlying genome organization in flies. *Nat. Commun.*, **9**, 189.
49. Carlson,M. (2019) org.Mm.eg.db: Genome wide annotation for Mouse. R package version 3.8.2.
50. Hinrichs,A.S., Karolchik,D., Baertsch,R., Barber,G.P., Bejerano,G., Clawson,H., Diekhans,M., Furey,T.S., Harte,R.A., Hsu,F. *et al.* (2006) The UCSC Genome Browser Database: update 2006. *Nucleic Acids Res.*, **34**, D590–D598.
51. Nicol,B., Grimm,S.A., Chalmel,F., Lecluze,E., Pannetier,M., Pailhoux,E., Dupin-De-Beyssat,E., Guiguen,Y., Capel,B. and Yao,H.H.C. (2019) RUNX1 maintains the identity of the fetal ovary through an interplay with FOXL2. *Nat. Commun.*, **10**, 5116.
52. Park,E.-S., Choi,S., Muse,K.N., Curry,T.E. and Jo,M. (2008) Response gene to complement 32 expression is induced by the luteinizing hormone (LH) surge and regulated by LH-induced mediators in the rodent ovary. *Endocrinology*, **149**, 3025–3036.
53. Kim,J., Sato,M., Li,Q., Lydon,J.P., DeMayo,F.J., Bagchi,I.C. and Bagchi,M.K. (2008) Peroxisome proliferator-activated receptor γ is a target of progesterone regulation in the preovulatory follicles and controls ovulation in mice. *Mol. Cell. Biol.*, **28**, 1770–1782.
54. Kim,J., Bagchi,I.C. and Bagchi,M.K. (2009) Signaling by hypoxia-inducible factors is critical for ovulation in mice. *Endocrinology*, **150**, 3392–3400.
55. Sharma,S.C. and Richards,J.S. (2000) Regulation of AP1 (Jun/Fos) factor expression and activation in ovarian granulosa cells. Relation of JunD and Fra2 to terminal differentiation. *J. Biol. Chem.*, **275**, 33718–33728.
56. Jo,M. and Curry,T.E. Jr. (2006) Luteinizing hormone-induced RUNX1 regulates the expression of genes in granulosa cells of rat periovulatory follicles. *Mol. Endocrinol.*, **20**, 2156–2172.
57. Park,E.-S., Park,J., Franceschi,R.T. and Jo,M. (2012) The role for runt related transcription factor 2 (RUNX2) as a transcriptional repressor in luteinizing granulosa cells. *Mol. Cell. Endocrinol.*, **362**, 165–175.
58. Bianco,S., Bellefleur,A.-M., Beaulieu,E., Beauparlant,C.J., Bertolin,K., Droit,A., Schoonjans,K., Murphy,B.D. and Gévry,N. (2019) The ovulatory signal precipitates LRH-1 transcriptional

switching mediated by differential chromatin accessibility. *Cell Rep.*, **28**, 2443–2454.
59. Fan,H.-Y., Liu,Z., Johnson,P.F. and Richards,J.S. (2011) CCAAT/enhancer-binding proteins (C/EBP)-α and -β are essential for ovulation, luteinization, and the expression of key target genes. *Mol. Endocrinol.*, **25**, 253–268.
60. Russell,D.L., Doyle,K.M.H., Gonzales-Robayna,I., Pipaon,C. and Richards,J.S. (2003) Egr-1 induction in rat granulosa cells by follicle-stimulating hormone and luteinizing hormone: combinatorial regulation by transcription factors cyclic adenosine 3′,5′-monophosphate regulatory element binding protein, serum response factor, Sp1, and early growth response factor-1. *Mol. Endocrinol.*, **17**, 520–533.
61. Puri,P., Little-Ihrig,L., Chandran,U., Law,N.C., Hunzicker-Dunn,M. and Zeleznik,A.J. (2016) Protein kinase A: a master kinase of granulosa cell differentiation. *Sci. Rep.*, **6**, 28132.
62. Kawate,H., Wu,Y., Ohnaka,K. and Takayanagi,R. (2007) Mutual transactivational repression of Runx2 and the androgen receptor by an impairment of their normal compartmentalization. *J. Steroid Biochem. Mol. Biol.*, **105**, 46–56.
63. Yang,R., Browne,J.A., Eggener,S.E., Leir,S.-H. and Harris,A. (2018) A novel transcriptional network for the androgen receptor in human epididymis epithelial cells. *Mol. Hum. Reprod.*, **24**, 433–443.
64. Ning,Y.-M. and Robins,D.M. (1999) AML3/CBFα1 is required for androgen-specific activation of the enhancer of the mouse sex-limited protein (Slp) gene. *J. Biol. Chem.*, **274**, 30624–30630.
65. Takayama,K.-i., Suzuki,T., Tsutsumi,S., Fujimura,T., Urano,T., Takahashi,S., Homma,Y., Aburatani,H. and Inoue,S. (2014) RUNX1, an androgen- and EZH2-regulated gene, has differential roles in AR-dependent and -independent prostate cancer. *Oncotarget*, **6**, 2263.
66. Stender,J.D., Kim,K., Charn,T.H., Komm,B., Chang,K.C.N., Kraus,W.L., Benner,C., Glass,C.K. and Katzenellenbogen,B.S. (2010) Genome-Wide Analysis of Estrogen Receptor α DNA Binding and Tethering Mechanisms Identifies Runx1 as a Novel Tethering Factor in Receptor-Mediated Transcriptional Activation. *Mol. Cell. Biol.*, **30**, 3943–3955.
67. Lee-Thacker,S., Jeon,H., Choi,Y., Taniuchi,I., Takarada,T., Yoneda,Y., Ko,C. and Jo,M. (2020) Core Binding Factors are essential for ovulation, luteinization, and female fertility in mice. *Sci. Rep.*, **10**, 9921.
68. Pierson Smela,M.D., Kramme,C.C., Fortuna,P.R.J., Adams,J.L., Su,R., Dong,E., Kobayashi,M., Brixi,G., Kavirayuni,V.S., Tysinger,E. *et al.* (2023) Directed differentiation of human iPSCs to functional ovarian granulosa-like cells via transcription factor overexpression. *Elife*, **12**, e83291.
69. Choi,Y., Jeon,H., Akin,J.W., Curry,T.E. Jr. and Jo,M. (2021) The FOS/AP-1 regulates metabolic changes and cholesterol synthesis in human periovulatory granulosa cells. *Endocrinology*, **162**.
70. Choi,Y., Rosewell,K.L., Brännström,M., Akin,J.W., Curry,T.E. Jr. and Jo,M. (2018) FOS, a critical downstream mediator of PGR and EGF signaling necessary for ovulatory prostaglandins in the human ovary. *J. Clin. Endocrinol. Metab.*, **103**, 4241–4252.
71. Astapova,O., Minor,B.M.N. and Hammes,S.R. (2019) Physiological and pathological androgen actions in the ovary. *Endocrinology*, **160**, 1166–1174.
72. Poulsen,L.C., Bøtkjær,J.A., Østrup,O., Petersen,K.B., Andersen,C.Y., Grøndahl,M.L. and Englund,A.L.M. (2020) Two waves of transcriptomic changes in periovulatory human granulosa cells. *Hum. Reprod.*, **35**, 1230–1245.
73. Tetsuka,M. and Hillier,S.G. (1997) Differential regulation of aromatase and androgen receptor in granulosa cells. *J. Steroid Biochem. Mol. Biol.*, **61**, 233–239.